



Innovative Applications of O.R.

# A mixed integer linear programming model for multi-satellite scheduling

Xiaoyu Chen<sup>a,b</sup>, Gerhard Reinelt<sup>b</sup>, Guangming Dai<sup>a,\*</sup>, Andreas Spitz<sup>b</sup><sup>a</sup> School of Computer Science, China University of Geosciences, Wuhan 430074, China<sup>b</sup> Institute of Computer Science, Heidelberg University, Heidelberg 69120, Germany

## ARTICLE INFO

### Article history:

Received 12 April 2018

Accepted 23 November 2018

Available online 26 November 2018

### Keywords:

Scheduling

Earth observing satellites

Integer programming

Mathematical programming

## ABSTRACT

We address the *multi-satellite scheduling problem with limited observation capacities* that arises from the need to observe a set of targets on the Earth's surface using imaging resources installed on a set of satellites. We define and analyze the conflict indicators of all available visible time windows of missions, as well as the feasible time intervals of resources. The problem is then formulated as a mixed integer linear programming model, in which constraints are derived from a careful analysis of the interdependency between feasible time intervals that are eligible for observations. We apply the proposed model to several different problem instances that reflect real-world situations. The computational results verify that our approach is effective for obtaining optimum solutions or solutions with a very good quality.

© 2018 Published by Elsevier B.V.

## 1. Introduction

Earth-observing satellites (EOS) are specially designed for the observation of activities or areas on the Earth's surface, and play an increasingly important role in resource explorations, disaster alerts, environmental damage analysis, and many other imaging demands (Liu, Laporte, Chen, & He, 2017). An EOS can photograph the target with a variety of equipped resources, such as sensors or cameras. Each resource has a limited observation region on the Earth's surface that is formed by the subpoint of the satellite's resource and the field of view. The observation activity can be controlled by the swing angle and the rotation angle of the resource (Habet, Vasquez, & Vimont, 2010; Liu, Bai, Chen, & Yao, 2014). Clearly, it is only possible for the resource to accomplish the observation if the target is visible to it (Mao, Xu, Hou, & Min, 2012).

During the observation process, every target has to be observed for a specified duration that depends on the resource, which can be calculated from the orbiting speed of the satellite and the scanning speed of the resource (Niu, Tang, Wu, Deng, & Zhai, 2015). The observation operation must be continuously and completely executed within a time window during which the target is visible to the satellite (Yao, Li, Bai, & He, 2010). For each mission, there may exist multiple feasible observation windows per resource.

Furthermore, some additional constraints may need to be taken into account, such as operational constraints of satellites, energy capacity restrictions, resource availability, or requirements of special resource types. Additionally, the swing angle and rotation angle of the resource must be set to point at the target. Thus, a setup time between two consecutive successful observations has to be considered to adjust the orientation of the resource (Mao et al., 2012). While the number of EOS is continuously increasing, so is the number of observation requests. Therefore, given the cost of operating satellites, it is reasonable to assume that the capacity of satellites to satisfy customer demands for observation missions is a scarce resource (Wu, Ma, Zhu, & Qiu, 2012), and that it may not be possible to satisfy all mission demands during a given observation period. Thus, the development of effective scheduling approaches is pertinent, such as the approach we discuss in the following.

In the following, we address the multi-satellite scheduling problem with limited observation capacities. In comparison to related work, we make four primary contributions. (1) We analyze the capacity of the resources and the distribution of visible time windows of missions. (2) We introduce and define conflict indicators of available visible time windows of missions. (3) We derive further constraints from a careful analysis of the interdependency of time intervals that are eligible for observations. (4) Finally, we formulate the problem as a mixed integer linear programming model. Our computational results indicate the effectiveness and efficiency of the proposed method.

The remainder of this paper is organized as follows. We first review the related work and the state-of-the-art in multi-satellite scheduling in Section 2. By defining the conflict indicator of all

\* Corresponding author.

E-mail addresses: [xiaoyu.chen@informatik.uni-heidelberg.de](mailto:xiaoyu.chen@informatik.uni-heidelberg.de) (X. Chen), [ip121@uni-heidelberg.de](mailto:ip121@uni-heidelberg.de) (G. Reinelt), [cugdgm@126.com](mailto:cugdgm@126.com) (G. Dai), [spitz@informatik.uni-heidelberg.de](mailto:spitz@informatik.uni-heidelberg.de) (A. Spitz).

available visible time windows of missions and by analyzing the capability of all feasible time intervals of resources, we formulate an exact mixed-integer linear program (MILP) in Section 3. Simulation results and a performance analysis on a series of benchmark problem instances are given in Section 4. Finally, a summary and our conclusions are provided in Section 5.

## 2. Related work

Given the complexity of the issue, a large portion of previous works is concerned with single satellite scheduling and address the efficient performance by providing an optimal solution and an upper bound. A common set of benchmark instances (S5-DPSP) of the satellite SPOT5 scheduling problem is proposed by Bensana, Lemaître, and Verfaillie (1999). Based on this data, a weighted acyclic digraph model is formulated by Gabrel and Vanderpooten (2002), and solved with a label-setting shortest path algorithm. Alternatively, formulations as generalized knapsack problems can be solved with a tabu search algorithm (Vasquez & Hao, 2001) or a genetic algorithm (Mansour & Dessouky, 2010). Two 0–1 linear programming models are considered by Gabrel (2006). Based on the valid inequalities that arise from node packing and the 3-regular independence system polyhedra, a strengthened formulation for the SPOT5 daily photograph scheduling is presented by Ribeiro, Constantino, and Lorena (2010). However, the benchmark instances are provided without consideration of the constraints that are imposed by a limited observation time of the target.

Wolfe and Sorensen (2000) propose a greedy algorithm and a genetic algorithm based on the assumption that there are only one resource and one observation window for every mission. A single-satellite single-orbit scheduling problem is addressed with a tabu search heuristic in (Cordeau & Laporte, 2005), an adaptive meta-heuristic in Liu et al. (2017), and a 0/1 linear programming model in (Sun, Wang, Xie, & Qin, 2010). Another 0/1 model based on pre-processing the observation segments is discussed by Jang, Choi, Bae, and Choi (2013). The problem of maximizing the total amount of downloaded data is addressed with a mixed-integer programming model and an iterative algorithm (Spangelo, Cutler, Gilson, & Cohn, 2015). There are also several publications that treat the single satellite scheduling as a machine scheduling problem with constraints of operating time windows. The problem is then solved by a heuristic (Barbulescu, Watson, & Whitley, 2004; Cheng, Ng, & Yuan, 2008; Lin, Liao, Liu, & Lee, 2005; Tangpattanakul, Nicolas, & Pierre, 2015). By considering the setup time between two consecutive observations, Lemaître, Verfaillie, Jouhaud, Lachiver, and Bataille (2002) introduce the selecting and scheduling problem for an agile Earth observation satellite. Dilkina and Havens (2005) take the limited time window and transition time constraints into account.

In comparison to the single satellite scheduling problem, the use of multiple satellites gives more flexibility and is thus more challenging (Spangelo et al., 2015). Wu, Liu, Ma, and Qiu (2013); Xiong, Leus, and Yang (2016); Zhang, Zhang, and Feng (2014) use graph representations to formulate the problem, for which dynamic programming and ant colony optimization algorithms are proposed to produce a near-optimal solution. To this end, simple sequential missions with conflicts can easily be represented as graphs. However, if the problem involves multiple satellites, the visibility fields of different resources may overlap. Furthermore, several targets may be in the field of view of the same resource simultaneously, and a target may be observed by more than one resource at the same time. Thus, the visible time windows are highly overlapping during the scheduling period, making the combinational characteristic of the problem more prominent. This ultimately

renders the uniform modelling of the problem difficult (Yao et al., 2010).

In order to decrease the complexity of the problem and improve computational efficiency, the multi-satellite scheduling problem is often decomposed into the primary problem of mission assignment and the sub-problem of single satellite scheduling (Wu et al., 2012; Yao et al., 2010). However, since each mission can be observed by multiple resources and since visible time windows interact, the decomposition approach is likely to become trapped in a local optimum of low quality. As a result, a series of mission merging strategies are studied Wang, Zhu, Yang, Zhu, and Ma (2015); Xu, Xu, Wang, and Peng (2010), and the multi-satellite scheduling for dynamic emergency missions is investigated Niu et al. (2015); Wang et al. (2015); Wang, Dai, and Vasile (2014). A multitude of different approaches have been investigated to address the problem, such as heuristics (e.g. greedy approaches (Bianchessi & Righini, 2008; Wang, Reinelt, Gao, & Tan, 2011) or local searches (Bonissone, Subbu, Eklund, & Kiehl, 2006)) and meta-heuristic algorithms (e.g. tabu searches (Bianchessi, Cordeau, Desrosiers, Laporte, & Raymond, 2007; Habet et al., 2010; Vasquez & Hao, 2003), genetic algorithms (Mao et al., 2012; Sun et al., 2010; Xhafa, Herrero, Barolli, Barolli, & Takizawa, 2013; Xhafa, Sun, & Barolli, 2012), evolutionary algorithms (Bonissone et al., 2006; Salman, Ahmad, & Omran, 2015), and simulated annealing algorithms (Xhafa et al., 2013; Yao et al., 2010)). While these optimization techniques show improvements towards obtaining the optimal or near-optimal solutions, they typically require extensive parameter tuning and cannot provide quality guarantees for the obtained solutions.

## 3. A mixed integer linear programming model

### 3.1. Problem description

In this section, we describe our mathematical programming model for the multi-satellite scheduling problem. We consider each mission as a point target that has to be observed continuously for a specified time by one of the resources of a satellite. An observation has to be carried out at a certain swing angle and a rotation angle of the resource. Therefore, a setup time between two consecutive observations of the same resource has to be taken into account. A mission requests a certain *imaging type* (visible, multispectral, infrared, or synthetic aperture radar), which must be provided by the corresponding resource. Of course, for modelling the problem, it is not necessary to know the location of the targets. We can determine beforehand at which times a target is visible to each resource and then schedule its observation accordingly. We first define the basic concepts that are used in the following.

**Definition 3.1. Visible Time Window.** A time interval during which the target is visible for the resource.

**Definition 3.2. Observation Time Window.** A time interval during which a given resource is assigned to a mission in the scheduling scheme.

**Definition 3.3. Feasible Time Interval.** A continuous time interval that is generated by the union of the overlapping visible time windows of a given resource.

**Definition 3.4. Conflict Degree.** The number of candidate missions that can be assigned to the same feasible time interval or subinterval.

The definitions are described in detail in Appendix A. Based on these concepts, we introduce the notation used in the following.

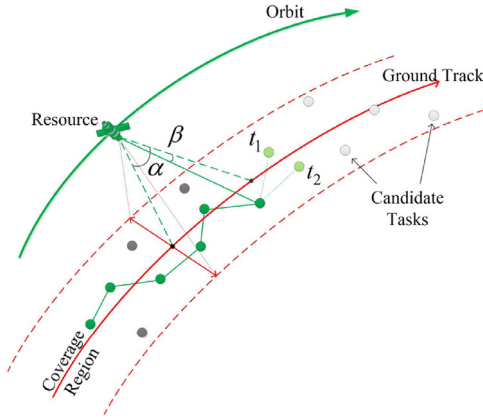


Fig. 1. Resource observation.

### 3.2. Notation

As the *scheduling period*, we denote the time interval during which observations can be scheduled, and write  $[S_{Beg}, S_{End}]$ , where  $S_{Beg} \geq 0$ .

The set of *missions* is denoted as  $\mathcal{M} = \{M_1, M_2, \dots, M_n\}$ . Each such mission  $M_i$  is specified by its earliest possible observation time  $E_i$ , its latest possible observation time  $L_i$ , and the requested duration  $D_i$  of the observation. Therefore, to satisfy the mission, a subinterval of length  $D_i$  has to be chosen in the time interval  $[E_i, L_i]$ . Every mission  $M_i$  has a positive weight  $w_i$  measuring its importance (the larger  $w_i$ , the more important the mission).

$\mathcal{R} = \{R_1, R_2, \dots, R_l\}$  is the set of *resources* (cameras, sensors) available on the various satellites. The maximum possible usage time of the resource  $R_j$  in the scheduling period is denoted as  $A_j$ .

The availability of resources for missions (in the scheduling period) is specified by appropriate visible time windows. For every resource  $R_j$  and every mission  $M_i$ , there is a set  $TW_{ij} = \{tw_{ij}^1, \dots, tw_{ij}^{n_{ij}}\}$  of  $n_{ij}$  *visible time windows* during which the resource can be used continuously for the mission. By determining the union of all overlapping visible time windows on resource  $R_j$  over the entire scheduling period, we can compute several disjoint *feasible time intervals* that can be assigned to missions. We denote them as  $RTW_j = \{rtw_j^1, \dots, rtw_j^{F_j}\}$  where  $F_j$  is the number of feasible time intervals of the resource  $R_j$ . It is obvious that, for all  $tw_{ij}^k$ ,  $M_i \in \mathcal{M}(R_j)$ ,  $k \in \mathcal{N}_{ij} = \{1, 2, \dots, n_{ij}\}$ , we have  $tw_{ij}^k \subseteq RTW_j$ . Each time window  $tw_{ij}^k$  is then given as  $tw_{ij}^k = [Beg_{ij}^k, End_{ij}^k]$ .

For a mission  $M_i \in \mathcal{M}$ , let  $\mathcal{R}(M_i) \subseteq \mathcal{R}$  be the set of resources that can be used for this mission. Let  $\mathcal{M}(R_j) \subseteq \mathcal{M}$  be the set of missions that a resource  $R_j \in \mathcal{R}$  can service.

The resource observation status is illustrated in Fig. 1. If resource  $R_j$  is used for observing mission  $M_i$ , then this has to happen with a certain *swing angle*  $\alpha$  and a *rotation angle*  $\beta$ . These angles are not constant but depend on the position of the resource and thus on the time  $t_i$  at which the observation for  $M_i$  starts within one of its feasible time windows. There are existing functions for computing these angles, which we denote as  $\alpha_{ijt_i}$  and  $\beta_{ijt_t}$ , respectively. A schematic overview of the functions is depicted in Fig. 2. Here, the elevation angle EL- $M_i$  and azimuth AZ- $M_i$  show angles  $\alpha_{ijt_t}$  and  $\beta_{ijt_t}$  for a mission  $M_i$  and the same resource  $R_j$ , depending on the start time  $t_i$  of the observation.

If two consecutive missions are to be carried out by the same resource, then a *setup time* has to be taken into account. The swing angle of resource  $R_j$  can be changed by  $\theta_j$  per second and, similarly, its rotation angle by  $\varphi_j$  per second. Furthermore, some time  $\delta_j$  is needed for stabilizing the resource after the angles are

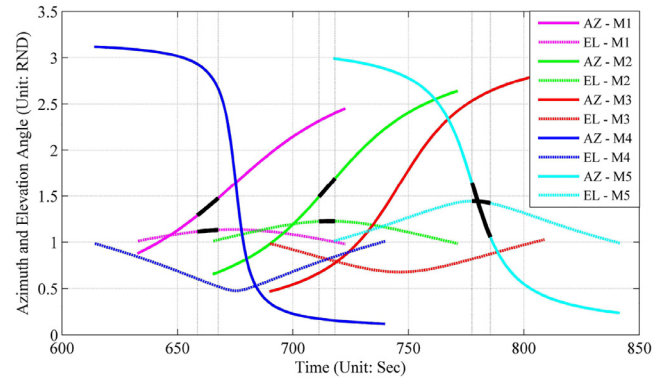


Fig. 2. Variation of swing and rotation angles.

adjusted. Angles cannot be adapted simultaneously, so if  $M_i$  and  $M_{i'}$  are two consecutive missions for  $R_j$ , then the time needed for changing to the correct position is

$$\mu_{it_i't_{i'}}^j = \frac{|\alpha_{i't_{i'}} - \alpha_{ijt_t}|}{\theta_j} + \frac{|\beta_{i't_{i'}} - \beta_{ijt_t}|}{\varphi_j} + \delta_j.$$

Of course,  $\mu_{it_i't_{i'}}^j \leq t_{i'} - t_i - D_i$  has to be satisfied.

We simplify the consideration of setup times by computing upper bounds. As we have  $\beta_{ij} \in [0, 2\pi)$  and  $\alpha_{ij} \in [-\alpha_j, \alpha_j]$  for some maximum angle  $\alpha_j$  depending on the resource, the maximum possible setup time between missions  $M_i$  and  $M_{i'}$  for  $R_j$  is  $\Delta_{i'i'}^j = \frac{2\alpha_j}{\theta_j} + \frac{\pi}{\varphi_j} + \delta_j$ .

### 3.3. Decision variables

For every mission  $M_i$  and every resource  $R_j$ , the binary variable  $x_{ij}^k$  specifies whether one of the available visible time windows ( $\mathcal{N}_{ij}$ ) is selected. We let  $x_{ij}^k = 1$  if the visible time window  $tw_{ij}^k$  is used. Otherwise, let  $x_{ij}^k = 0$ . For every mission  $M_i$ , we also have a continuous variable  $t_i$  that denotes the starting time of its observation.

### 3.4. Objective

Assuming that the resources are limited and that not all missions can be carried out, our objective is to schedule either as many missions as possible, i.e.,

$$\max \sum_{M_i \in \mathcal{M}} \sum_{R_j \in \mathcal{R}(M_i)} \sum_{k \in \mathcal{N}_{ij}} x_{ij}^k,$$

or to maximize the total weight of accomplished missions, i.e.,

$$\max \sum_{M_i \in \mathcal{M}} \sum_{R_j \in \mathcal{R}(M_i)} \sum_{k \in \mathcal{N}_{ij}} w_i x_{ij}^k.$$

### 3.5. Constraints

In the following, let  $U$  denote a large number depending on the scheduling period (i.e. it serves as the “Big-M” required for modelling logical implications).

*Mission accomplishment.* It is unlikely that every mission can be carried out. Therefore, although one target can be observed by several resources, the profit of each target counts at most once. For every mission  $M_i \in \mathcal{M}$ , we thus have

$$\sum_{R_j \in \mathcal{R}(M_i)} \sum_{k \in \mathcal{N}_{ij}} x_{ij}^k \leq 1.$$

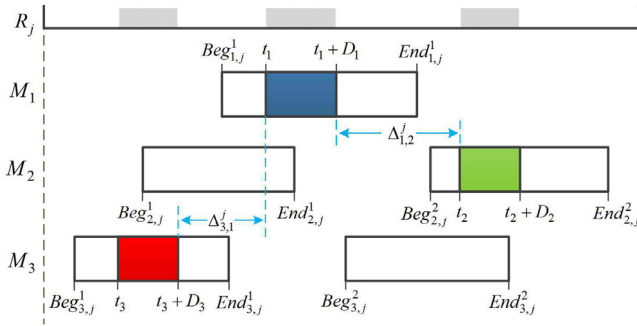


Fig. 3. Observation time window constraint.

**Maximum usage time.** The total observation time in the scheduling period that can be scheduled for a resource is bounded by the given maximum observation time. So for every  $R_j \in \mathcal{R}$ , we have the inequality

$$\sum_{M_i \in \mathcal{M}(R_j)} \sum_{k \in \mathcal{N}_{ij}} D_i \cdot x_{ij}^k \leq A_j.$$

**Feasibility of observation time.** For each  $M_i \in \mathcal{M}$  we have

$$\begin{aligned} t_i &\geq S_{\text{Beg}} \\ t_i + D_i &\leq S_{\text{End}}. \end{aligned}$$

**3.5.0.4. Observation window.** If resource  $R_j$  and time window  $tw_{ij}^k$  for mission  $M_i$  have been selected, then the observation activity has to be placed completely within this interval. This is modeled by the following constraints for all  $M_i \in \mathcal{M}$  and every  $R_j \in \mathcal{R}(M_i)$ ,  $k \in \mathcal{N}_{ij}$ :

$$\begin{aligned} t_i - \text{Beg}_{ij}^k \cdot x_{ij}^k &\geq 0, \\ t_i - (\text{End}_{ij}^k - D_i) \cdot x_{ij}^k - U \cdot (1 - x_{ij}^k) &\leq 0. \end{aligned}$$

**Setup time.** A minimum transition time for achieving the correct position has to be considered between each pair of consecutive observation activities of the same resource. This situation is depicted in Fig. 3.

Thus, for all  $R_j \in \mathcal{R}$  and any pair of observations  $M_i, M_{i'} \in \mathcal{M}(R_j)$ , if both missions  $M_i$  and  $M_{i'}$  have been assigned to be carried out by  $R_j$  then either  $t_i \geq t_{i'} + D_{i'} + \Delta_{i,i'}^j$  or  $t_{i'} \geq t_i + D_i + \Delta_{i,i'}^j$  has to hold.

For modelling this constraint, we introduce binary variables  $f_{i,i'}^j$  and  $f_{i',i}^j$ , where  $f_{i,i'}^j = 1$  ( $f_{i',i}^j = 1$ ) if and only if both  $M_i$  and  $M_{i'}$  are carried out by  $R_j$  and  $M_i$  is observed after  $M_{i'}$  ( $M_{i'}$  is observed after  $M_i$ ). Since  $f_{i,i'}^j + f_{i',i}^j = \sum_k x_{ij}^k \cdot \sum_{k'} x_{i'j}^{k'}$ , the disjunction can then be expressed as

$$\begin{aligned} t_i - t_{i'} &\geq (D_{i'} + \Delta_{i,i'}^j) \cdot f_{i,i'}^j - (U - D_{i'}) \cdot (1 - f_{i,i'}^j) \\ t_{i'} - t_i &\geq (D_i + \Delta_{i',i}^j) \cdot f_{i',i}^j - (U - D_i) \cdot (1 - f_{i',i}^j). \end{aligned}$$

For a consistent setting of the new variables, we need

$$\begin{aligned} f_{i,i'}^j + f_{i',i}^j &\leq \sum_{k \in \mathcal{N}_{ij}} x_{ij}^k, \\ f_{i,i'}^j + f_{i',i}^j &\leq \sum_{k' \in \mathcal{N}_{i'j}} x_{i'j}^{k'}, \\ f_{i,i'}^j + f_{i',i}^j &\geq \sum_{k \in \mathcal{N}_{ij}} x_{ij}^k + \sum_{k' \in \mathcal{N}_{i'j}} x_{i'j}^{k'} - 1, \\ \sum_{R_j \in \mathcal{R}(M_i) \cap \mathcal{R}(M_{i'})} (f_{i,i'}^j + f_{i',i}^j) &\leq 1. \end{aligned}$$

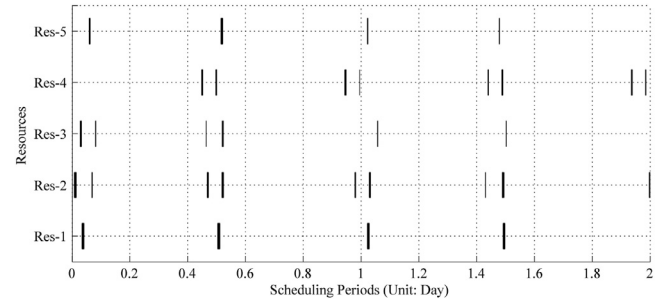


Fig. 4. Distribution of feasible time intervals.

**Resource feasibility.** Motivated by the definitions of the *feasible time interval* and the *conflict degree* (also see Appendix A), we consider resource feasibility as a constraint. For a *feasible time interval*  $rtw_j^k$  on  $R_j$ , all *effective feasible time subintervals*  $srtw_j^{kl} \subset rtw_j^k$  are also considered according to the contention conflict degree. In fact, it is a continuous time subinterval within which the visible time windows are highly overlapping and not all of the corresponding candidate missions can be accomplished in  $srtw_j^{kl}$ . We calculate how many missions can at most be assigned to a subinterval  $srtw_j^{kl}$ , and denote them as  $srn_j^{kl}$ . For each such effective feasible time subinterval  $srtw_j^{kl}$ , we have inequalities

$$\begin{aligned} \sum_{M_i \in \mathcal{M}(R_j)} \sum_{k' \in \mathcal{N}_{ij}} x_{ij}^{k'} &\leq srn_j^{kl} \\ \sum_{M_i \in \mathcal{M}(R_j)} \sum_{k' \in \mathcal{N}_{ij}} (D_i + \delta_j) \cdot x_{ij}^{k'} &\leq |srtw_j^{kl}| + \delta_j, \end{aligned}$$

where  $tw_{ij}^{k'} \subset srtw_j^{kl}$ .

The generation of the effective feasible time subinterval  $srtw_j^{kl}$  and the computation of the corresponding maximum assignment capacity  $srn_j^{kl}$  are described in detail in Appendix B. All operations with respect to the resource feasibility are computed in preprocessing, and the computation results are regarded as constraints in modelling. Furthermore, these newly proposed formulations are a set of effective inequalities and produce a significant improvement in obtaining a tighter upper bound of instances.

**Integrity constraints.** For all  $M_i \in \mathcal{M}$ , all  $R_j \in \mathcal{R}(M_i)$ , and all  $k \in \mathcal{N}_{ij}$  we have

$$x_{ij}^k \in \{0, 1\}.$$

### 3.6. Improved constraints

A mission may have several disjoint visible time windows for each resource and the fraction of the time window that is needed for observation may be comparatively small. Fig. 4 illustrates the distribution of all feasible time intervals over time. We find that the availability distribution of resources is quite sparse over the entire scheduling period.

In the first model, the value of  $t_i$  is always feasible for the entire scheduling period due to the introduction of  $U$  as “Big-M”. Typically, for large values of  $U$ , this is an obstacle for obtaining a good bound from the LP relaxation. Thus, we avoid the use of  $U$  by defining new (continuous) variables  $t_{ij}^k$  that denote the starting time of mission  $M_i$  if  $x_{ij}^k$  is selected. As bounds we then have  $t_{ij}^k \geq S_{\text{Beg}}$  and  $t_{ij}^k + D_i \leq S_{\text{End}}$ . Based on this deliberation, new constraints are introduced as follows.



**Table 1**  
Test instances.

Instance	Period	$ \mathcal{R} $	$ \mathcal{M} $	$\sum w_i$	Instance	Period	$ \mathcal{R} $	$ \mathcal{M} $	$\sum w_i$
M-1	24 H	3	C100	621	C-1	24 H	3	M100	620
M-2	24 H	3	C200	1191	C-2	24 H	3	M200	1218
M-3	24 H	3	C300	1790	C-3	24 H	3	M300	1785
M-4	24 H	5	C100	621	C-4	24 H	5	M100	620
M-5	24 H	5	C200	1191	C-5	24 H	5	M200	1218
M-6	24 H	5	C300	1790	C-6	24 H	5	M300	1785
M-7	24 H	5	C400	2401	C-7	24 H	5	M400	2385
M-8	24 H	5	C500	2976	C-8	24 H	5	M500	2998
M-9	48 H	5	C100	621	C-9	48 H	5	M100	620
M-10	48 H	5	C200	1191	C-10	48 H	5	M200	1218
M-11	48 H	5	C300	1790	C-11	48 H	5	M300	1785
M-12	48 H	5	C400	2401	C-12	48 H	5	M400	2385
M-13	48 H	5	C500	2976	C-13	48 H	5	M500	2998
R-1	24 H	4	R300	1821	R-7	24 H	6	R600	3617
R-2	24 H	4	R400	2427	R-8	24 H	6	R700	4193
R-3	24 H	4	R500	3004	R-9	24 H	6	R800	4783
R-4	24 H	6	R300	1821	R-10	24 H	6	R900	5371
R-5	24 H	6	R400	2427	R-11	24 H	6	R1000	5987
R-6	24H	6	R500	3004					

**Observation window.** If the resource  $R_j$  and a corresponding visible time window  $tw_{ij}^k$  for mission  $M_i$  have been selected, then the observation has to be completely placed within this interval. For all  $M_i \in \mathcal{M}$  and  $R_j \in \mathcal{R}(M_i)$ ,  $k \in \mathcal{N}_{ij}$ , we thus have

$$t_{ij}^k - Beg_{ij}^k \cdot x_{ij}^k \geq 0,$$

$$t_{ij}^k - (End_{ij}^k - D_i) \cdot x_{ij}^k \leq 0.$$

**Setup time.** For all resources  $R_j$  and any pair of observations  $M_i, M_{i'} \in \mathcal{M}(R_j)$ , if both missions  $M_i$  and  $M_{i'}$  have been assigned to be carried out by  $R_j$ , then we obtain tighter constraints for the respective starting times since either  $(D_{i'} + \Delta_{i'j}^j) \leq t_{ij}^k - t_{i'j}^{k'} \leq End_{ij}^k - D_i - Beg_{i'j}^{k'}$  or  $(D_i + \Delta_{ij}^j) \leq t_{i'j}^{k'} - t_{ij}^k \leq End_{i'j}^{k'} - D_{i'} - Beg_{ij}^k$ . Here, we distinguish three cases.

1. For resource  $R_j$ , if the candidate visible time windows  $tw_{ij}^k$  and  $tw_{i'j}^{k'}$  are potentially “ordered” and satisfy that  $End_{ij}^k - D_i - Beg_{i'j}^{k'} < \Delta_{i'j}^j$  (that is, if both of them are assigned, then mission  $M_i$  will definitely be executed before mission  $M_{i'}$ ), we have
2. For resource  $R_j$ , if the candidate visible time windows  $tw_{i'j}^{k'}$  and  $tw_{ij}^k$  are potentially “ordered” and satisfy that  $End_{i'j}^{k'} - D_{i'} - Beg_{ij}^k < \Delta_{ij}^j$  (that is, if both of them are assigned, then mission  $M_{i'}$  will definitely be executed before mission  $M_i$ ), we have
3. Only if the candidate visible time windows  $tw_{ij}^k$  and  $tw_{i'j}^{k'}$  are overlapping we introduce binary variables  $f_{jii'}^{kk'}$  and  $f_{jji'}^{k'k}$ , where  $f_{jii'}^{kk'} = 1$  if  $M_i$  is observed after  $M_{i'}$  and  $f_{jji'}^{k'k} = 1$  if  $M_{i'}$  is observed after  $M_i$  (by  $R_j$ ). Since  $f_{jii'}^{kk'} + f_{jji'}^{k'k} = x_{ij}^k \cdot x_{i'j}^{k'}$ , the disjunction can be expressed as

$$t_{ij}^k - t_{i'j}^{k'} \geq (D_{i'} + \Delta_{i'j}^j) \cdot f_{jii'}^{kk'} - (End_{i'j}^{k'} - D_{i'} - Beg_{ij}^k \cdot f_{jji'}^{k'k}) \cdot (1 - f_{jii'}^{kk'}),$$

$$t_{i'j}^{k'} - t_{ij}^k \geq (D_i + \Delta_{ij}^j) \cdot f_{jji'}^{k'k} - (End_{ij}^k - D_i - Beg_{i'j}^{k'} \cdot f_{jii'}^{kk'}) \cdot (1 - f_{jji'}^{k'k}),$$

or equivalently as

$$t_{ij}^k - t_{i'j}^{k'} \geq (End_{i'j}^{k'} + \Delta_{i'j}^j) \cdot f_{jii'}^{kk'} + Beg_{ij}^k \cdot f_{jji'}^{k'k} - (End_{i'j}^{k'} - D_{i'}),$$

$$t_{i'j}^{k'} - t_{ij}^k \geq (End_{ij}^k + \Delta_{ij}^j) \cdot f_{jji'}^{k'k} + Beg_{i'j}^{k'} \cdot f_{jii'}^{kk'} - (End_{ij}^k - D_i).$$

For the consistent setting of the new binary variables we need

$$f_{jii'}^{kk'} + f_{jji'}^{k'k} \leq x_{ij}^k$$

$$f_{jii'}^{kk'} + f_{jji'}^{k'k} \leq x_{i'j}^{k'}$$

$$f_{jii'}^{kk'} + f_{jji'}^{k'k} \geq x_{ij}^k + x_{i'j}^{k'} - 1$$

$$\sum_{R_j \in \mathcal{R}(M_i) \cap \mathcal{R}(M_{i'})} \sum_{k \in \mathcal{N}_{ij}} \sum_{k' \in \mathcal{N}_{i'j}} (f_{jii'}^{kk'} + f_{jji'}^{k'k}) \leq 1.$$

With the introduction of these variables, we do not have  $U$  (serving as “Big-M”) anymore. Instead, additional 5-index variables are introduced for pairs of overlapping visible time windows. However, for real-world problem instances where there are many visible time windows for the missions, the number of additional variables is acceptable. We give a detailed analysis in [Section 4.2](#). The newly introduced constraints also help to reformulate the conflict segments pairs, hence decreasing the number of binary variables in the model ([Jang et al., 2013](#)), while simultaneously eliminating the “Big-M” in formulating the satellite range scheduling problem ([Luo, Wang, Li, & Li, 2017](#)).

#### 4. Computational experiments

In the following, we describe our experiments on several test instances.

##### 4.1. Test instances

For analyzing the performance of our model, we generate several test instances. We use the current on-orbit environment and disaster monitoring satellites HJ-1A, HJ-1B, and HJ-1C, which can carry out large-scale, all-weather, and 24 hours dynamic monitoring for the ecological environment and disaster. The satellite HJ-1A is equipped with a CCD scanner and a hyperspectral imager, HJ-1B is equipped with a CCD scanner and an infrared scanner, and HJ-1C is equipped with an s-wave band synthetic aperture radar that has two working modes. The satellites HJ-1A and HJ-1B are located about 650 kilometre above the Earth’s surface

**Table 2**  
Model information.

MILP	Decision Variables	$x_{ij}^k \in \{0, 1\}$ $t_i \in \mathbb{R}$	$M_i \in \mathcal{M}$ , all $R_j \in \mathcal{R}(M_i)$ , and all $k \in \mathcal{N}_{ij}$ $M_i \in \mathcal{M}$
	Introduced Variables	$f_{ij}^j \in \{0, 1\}$ $f_{ji}^i \in \{0, 1\}$	$M_i, M_{i'} \in \mathcal{M}$ , all $R_j \in \mathcal{R}(M_i) \cap \mathcal{R}(M_{i'})$
Improved MILP	Decision Variables	$x_{ij}^k \in \{0, 1\}$ $t_{ij}^k \in \mathbb{R}$	$M_i \in \mathcal{M}$ , all $R_j \in \mathcal{R}(M_i)$ , and all $k \in \mathcal{N}_{ij}$
	Introduced Variables	$f_{ji}^{kk'} \in \{0, 1\}$ $f_{ji}^{kk} \in \{0, 1\}$	$M_i, M_{i'} \in \mathcal{M}$ , all $R_j \in \mathcal{R}(M_i) \cap \mathcal{R}(M_{i'})$ all $k \in \mathcal{N}_{ij}$ and $k' \in \mathcal{N}_{i'j}$ $tw_{ij}^k$ and $tw_{i'j}^{k'}$ are overlapped.

**Table 3**  
Model information.

Ins.	$n'$	MILP			Improved MILP		
		mVC	mVB	mC	mVC	mVB	mC
C-1	0	100	4082	10,463	100	1838	7713
C-2	6	194	15,234	38,620	218	3456	20510
C-3	2	298	36,466	92,019	360	8794	53973
C-4	2	98	8071	20,595	189	3543	14114
C-5	6	194	38,744	97,831	454	7176	44853
C-6	2	298	78,881	198,598	701	17349	106032
C-7	15	385	129,662	326,594	992	27780	192205
C-8	13	487	198,407	499,268	1265	45169	311769
C-9	3	97	9378	24,157	354	7280	35404
C-10	7	193	50,217	126,800	667	11945	92045
C-11	3	297	116,704	293,764	1098	30796	235087
C-12	18	382	218,518	550,073	1664	43784	463025
C-13	16	484	345,330	868,124	2086	67448	724176
M-1	17	83	2969	7626	83	1453	5964
M-2	18	182	13,938	35,388	206	3308	19270
M-3	27	273	32,290	81,562	320	8278	47707
M-4	19	81	5922	15,125	158	2916	11260
M-5	19	181	31,354	79,275	414	6738	39564
M-6	29	271	72,947	183,759	643	16907	97369
M-7	50	350	152,005	382,102	797	16431	136066
M-8	93	407	182,919	459,547	885	17681	158157
M-9	19	81	7977	20,519	313	6263	30347
M-10	22	178	51,349	129,772	721	13201	103415
M-11	31	269	123,785	311,638	1119	31573	247473
M-12	64	336	221,047	556,076	1323	26747	328150
M-13	118	382	283,211	711,799	1525	29387	415919
R-1	125	175	13,765	34,892	227	3321	21800
R-2	181	219	21,159	53,458	273	4419	30080
R-3	237	263	29,208	73,625	324	4638	36312
R-4	125	175	28,598	72,309	438	6206	40462
R-5	181	219	45,265	114,097	533	8493	57609
R-6	237	263	63,593	159,954	631	8895	70923
R-7	284	316	92,423	232,641	829	11651	112816
R-8	305	395	148,393	373,188	1079	15525	180564
R-9	347	453	215,280	540854	1342	16974	263464
R-10	379	521	279,252	701080	1514	17806	324658
R-11	389	611	405,523	1017699	1819	22687	461934

in a sun-synchronous orbit with 14.737 orbits per day. The satellite HJ-1C is located about 500km above the Earth's surface in a sun-synchronous orbit with 15.22 orbits per day. The resources on satellites HJ-1A and HJ-1B can observe the complete surface of the Earth in 2 days. Three types R, M, and C of spot target sets are generated with different resource conflict characteristics.

R Targets are generated randomly and uniformly distributed over the entire land-area on Earth.

C All targets are randomly generated in clusters over the entire land-area on Earth.

M Targets with a high number of conflicts are generated manually and clustered over several regions on Earth.

The observation times  $D_i$  for the missions are integers that are generated uniformly from the interval [3,10]. If weights  $w_i$  are

taken into account, they are integers that are generated uniformly from [1,10].

Table 1 shows a summary of the generated test instances. The hypothetical start time of the scheduling period is 2016-06-01 06:00:00. The scheduling horizon is 24 or 48 hours. By combining different satellites and target sets, 37 problem instances are generated.

Further details on all instances are provided in Appendix C. By computing some characteristic numbers, we quantify the availability of resources and the complexity of instances. We calculate the maximum possible number of missions ( $m$ ) that can be assigned to a resource according to constraint (Barbulescu et al., 2004). It is given as the sum of  $m_j^k$  of feasible time intervals of the resource  $R_j$ . Furthermore, we introduce the resource contention degree ( $conf$ ), which reflects the limitation of each feasible time interval of

**Table 4**

Optimization results: number of missions.

Ins.	Objective: Maximize the total number of assigned missions							
	Produced by the MILP				Produced by the Improved MILP			
	Root/Final upper bound	Best Result	Gap	Run time(second)	Root/Final upper bound	Best Result	Gap	Run time(second)
C-1	26.00/26	26	0.00%	0	26.00/26	26	0.00%	0
C-2	82.00/82	82	0.00%	19	82.00/82	82	0.00%	0
C-3	85.89/85	85	0.00%	265	85.00/85	85	0.00%	1
C-4	44.00/44	44	0.00%	23	44.00/44	44	0.00%	2
C-5	129.84/128	126	1.56%	–	130.84/129	128	0.78%	–
C-6	133.00/133	125	6.02%	–	132.00/131	131	0.00%	683
C-7	163.98/163	157	3.68%	–	164.98/163	162	0.61%	–
C-8	181.55/179	125	30.17%	–	183.85/179	178	0.56%	–
C-9	73.76/72	71	1.39%	–	73.76/72	72	0.00%	157
C-10	155.84/155	121	21.94%	–	157.84/155	155	0.00%	377
C-11	178.00/178	132	25.84%	–	178.00/176	175	0.57%	–
C-12	265.79/265	160	<b>39.62%</b>	–	266.79/265	259	2.26%	–
C-13	291.97/290	180	37.93%	–	293.97/290	285	1.72%	–
M-1	39.00/39	39	0.00%	2	39.00/39	39	0.00%	0
M-2	86.00/86	86	0.00%	15	86.00/86	86	0.00%	1
M-3	108.00/107	107	0.00%	153	108.00/107	107	0.00%	8
M-4	53.00/53	53	0.00%	17	53.00/53	53	0.00%	1
M-5	124.00/124	121	2.42%	–	123.00/122	122	0.00%	139
M-6	151.00/151	143	5.30%	–	150.00/150	149	0.67%	–
M-7	228.93/225	197	12.44%	–	227.93 /224	223	0.45%	–
M-8	309.81/305	282	7.54%	–	308.81 /304	303	0.33%	–
M-9	82.92/81	81	0.00%	1581	82.92/81	81	0.00%	25
M-10	162.99/162	138	14.81%	–	162.99/162	161	0.62%	–
M-11	206.00/206	158	23.30%	–	206.00/205	204	0.49%	–
M-12	305.88/301	218	27.57%	–	304.88/301	296	1.66%	–
M-13	402.00/402	294	26.87%	–	403.99/401	391	<b>2.49%</b>	–
R-1	210.92/209	209	0.00%	118	209.00/209	209	0.00%	1
R-2	287.92/286	286	0.00%	113	286.00/286	286	0.00%	1
R-3	381.00/380	380	0.00%	223	380.00/380	380	0.00%	1
R-4	239.82/238	236	0.84%	–	238.75/237	236	0.42%	–
R-5	317.82/316	314	0.63%	–	315.94/315	314	0.32%	–
R-6	412.00/411	409	0.49%	–	410.94/410	409	0.24%	–
R-7	507.00/507	434	14.40%	–	506.99 /505	502	0.59%	–
R-8	581.83/581	497	14.46%	–	583.83 /580	579	0.17%	–
R-9	682.83/682	593	13.05%	–	682.83 /679	677	0.29%	–
R-10	763.83/763	670	12.19%	–	765.83 /762	760	0.26%	–
R-11	–/–	–	–	–	839.33 /835	833	0.24%	–

resources, as well as the average conflict degree of missions, which is calculated as  $conf_j = \frac{T_j - F_j}{F_j}$ . Intuitively, it denotes how many missions can be assigned synchronously to a resource during the entire scheduling period, while  $conf_j = 0$  indicates that there is no resource contention conflict. These two conflict indicators illustrate the potential complexity of the instance when assigning resources to missions.

In comparison to  $N$ ,  $m$  decreases quickly for higher values of  $conf$ , indicating a more exact upper bound. Additionally, the potential assignment opportunity of missions denotes the flexibility in assigning a resource along with an observation time to a mission (including the average number of visible time windows of a mission ( $paon$ ) and the average visible time of a mission ( $paot$ )). Here, it is obvious that even if two missions have the same total visible time duration, it is more difficult to assign the mission that has the higher number of visible time windows.

#### 4.2. Comparison of proposed models

A summary of the decision variables used in the different formulations is shown in Table 2.

Furthermore, we investigate the effect of the preprocessing step (i.e., the reduction of the size of the search space) and compare the proposed models over different instances (i.e., the number of variables and constraints of a model). The results are shown in

detail in Table 3 and indicate an improvement of each phase in the overall performance of the proposed method.

In Table 3,  $n'$  denotes the number of missions that are scheduled during preprocessing. It is calculated based on the *effective feasible time subinterval* (see Appendix B). With  $mVC$ ,  $mVB$ , and  $mC$ , we denote the number of continuous variables, the number of binary variables, and the number of constraints, respectively. The results show that the preprocessing is especially effective for instances with randomly distributed targets  $\mathcal{R}$ . In the MILP, the number of continuous variables equals the number of missions, and the number of binary variables exponentially increases with the number of missions, meaning that  $mVC = n - n'$  and  $mVB \approx (n - n')^2$ . In contrast, for the improved MILP, the number of continuous variables equals the number of visible time windows, meaning that  $mVC = (n - n') \cdot paon$ . Due to the linearization of the formulation, the binary variable is introduced only if the two candidate visible time windows are overlapping. Thus, compared to the MILP, the number of binary variables is smaller, especially for the instance  $C$  of target sets (see Table C.6), where  $mVB \ll (n - n')^2$ .

#### 4.3. Optimization results

We test our model on all instances with Gurobi 6.5.1 on a 3.40 Gigahertz PC with 16 Gigabyte RAM and 8 cores. The maximum run time is set to 6 hours. Both objective functions, i.e., maximizing the number of scheduled missions as well as maximizing

**Table 5**

Optimization results: weight of missions.

Ins.	Objective: Maximize the total weight of assigned missions							
	Produced by the MILP				Produced by the Improved MILP			
	Root/Final upper bound	Best Result	Gap	Run time(second)	Root/Final upper bound	Best Result	Gap	Run time(second)
C-1	194.72/194	194	0.00%	1	194.71/194	194	0.00%	0
C-2	600.62/599	599	0.00%	8	600.61/599	599	0.00%	1
C-3	643.35/629	629	0.00%	68	631.88/629	629	0.00%	3
C-4	334.01/318	318	0.00%	375	334.01/318	318	0.00%	39
C-5	903.61/894	881	1.45%	–	899.58/888	887	0.11%	–
C-6	951.06/939	928	1.17%	–	946.05/928	928	0.00%	509
C-7	1211.39/1199	1132	5.59%	–	1218.36/1198	1174	2.00%	–
C-8	1364.65/1351	1300	3.77%	–	1374.62/1348	1329	1.41%	–
C-9	504.71/499	492	1.40%	–	504.71/495	495	0.00%	912
C-10	1048.39/1042	1024	1.73%	–	1055.39/1042	1038	0.38%	–
C-11	1243.76/1239	1162	6.21%	–	1243.76/1226	1219	0.57%	–
C-12	1799.62/1793	1148	35.97%	–	1806.59/1787	1735	2.91%	–
C-13	2050.11/2050	1353	34.00%	–	2060.03/2034	1974	<b>2.95%</b>	–
M-1	275.35/269	269	0.00%	5	272.04/269	269	0.00%	0
M-2	586.78/578	578	0.00%	60	590.40/578	578	0.00%	9
M-3	745.00/728	728	0.00%	496	739.31/728	728	0.00%	71
M-4	386.65/375	375	0.00%	51	382.50/375	375	0.00%	18
M-5	831.44/818	783	4.28%	–	823.26/807	800	0.87%	–
M-6	1031.35/1018	982	3.54%	–	1026.34/1009	1001	0.79%	–
M-7	1558.55/1536	1510	1.69%	–	1554.54/1533	1523	0.65%	–
M-8	2037.25/2017	1964	2.63%	–	2033.24/2008	1995	0.65%	–
M-9	550.25/541	540	0.18%	–	550.24/540	540	0.00%	49
M-10	1042.59/1041	969	6.92%	–	1042.59/1036	1024	1.16%	–
M-11	1371.50/1367	1059	22.53%	–	1371.49/1360	1337	1.69%	–
M-12	1981.15/1977	1627	17.70%	–	1989.14/1970	1944	1.32%	–
M-13	2552.34/2552	1746	31.58%	–	2560.33/2544	2475	2.71%	–
R-1	1344.55/1329	1329	0.00%	263	1332.42/1329	1329	0.00%	10
R-2	1816.51/1806	1806	0.00%	230	1809.70/1806	1806	0.00%	23
R-3	2366.41/2355	2355	0.00%	671	2358.70/2355	2355	0.00%	8
R-4	1550.02/1538	1520	1.17%	–	1544.75/1528	1520	0.52%	–
R-5	2039.12/2025	2006	0.94%	–	2028.58/2015	2006	0.45%	–
R-6	2581.86/2572	2552	0.78%	–	2581.58/2568	2559	0.35%	–
R-7	3171.19/3168	2835	10.51%	–	3170.75/3157	3142	0.48%	–
R-8	3635.33/3635	2984	17.91%	–	3639.34/3621	3595	0.72%	–
R-9	4217.33/4215	3533	16.18%	–	4223.28/4204	4177	0.64%	–
R-10	4700.81/4700	3984	15.23%	–	4708.87/4688	4659	0.62%	–
R-11	–/–	–	–	–	5189.80/5165	5125	0.77%	–

the total weights of scheduled missions, are considered. The results are shown in Tables 4 and 5, respectively. For each instance, we show the *root upper bound*, the *final upper bound* found by the Gurobi, and the value of the *best solution found*. If the running time is not exceeded, then the latter two are equal and represent the optimum value. The *gap* is computed as  $(\text{final upper bound} - \text{best solution})/\text{final upper bound}$ . The CPU time is shown if the optimum is found in less than 6 hours.

In Table 4, we see that in comparison to the results produced by the MILP, a larger number of optimal solutions can be obtained by the improved MILP. For most of the problem instances, the tightest upper bounds can be efficiently generated by the improved MILP. Optimal solutions are usually obtained in less than 1000 second. Within 6 hours, solutions with a small optimality gap can be determined. The worst gap among all results is 2.49% for the improved model, whereas the worst generated gap among results produced by the MILP is 39.62%. The MILP also fails to obtain a feasible solution for instance R-11. In combination with Table 3, these findings indicate that the performance of the proposed models varies with the size of the instance. The advantages are similar to those obtained when maximizing the total weights of assigned missions shown in Table 5. Here, the worst gap produced by the improved MILP is 2.95%, while the worst gap produced by the MILP is 35.97%.

These results can be improved further if we let Gurobi run for more than 6 hours. For example, for instance M-11, we can obtain the optimal solution with 205 assigned missions in 41,924 second,

and a better solution with a total weight for assigned missions of 1340 in 35,523 s with a gap of 1.47%.

To directly compare instances, consider instances C-13 and M-13, which have the same available resources and the same number of missions for a scheduling horizon of 2 days. Both in the MILP and the improved MILP, the potential assignment opportunities *paon* and *paot* of missions for instance C-13 are higher than for instance M-13. This reflects that the improved model is more flexible in assigning a resource and an observation time to a mission. The size of the model scale of instance C-13 is slightly larger than that of instance M-13. Furthermore, for the improved MILP, the conflict indicator *conf* of instance C-13 is larger than that of instance M-13, meaning that the size of the model scale of the instance C-13 is much bigger than that of the instance M-13.

In Fig. 5, we show further details about the problems and the optimization process. For instances with different computational complexity and different contention conflict for resources, the first column of the graph shows the potential capacity of resources for providing an upper bound as well as the performance of the proposed model for providing an optimal solution. The maximum accomplishment rate of missions and the best results that Gurobi achieves are represented on the left of Fig. 5, respectively. The following three columns on the right of Fig. 5 show the gap of the best solution obtained so far versus the runtime, and indicate that good upper bounds can be obtained fairly quickly.



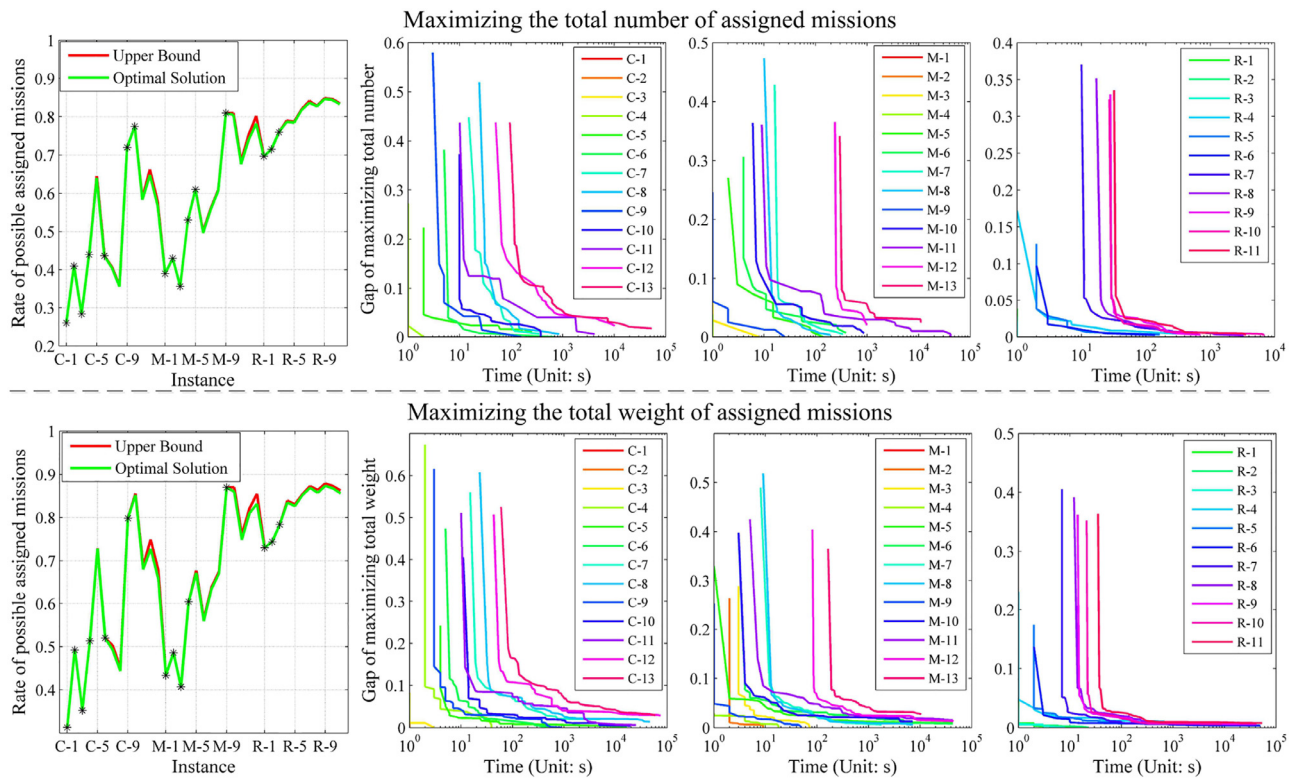


Fig. 5. Optimization results and the variation of computational efficiency. (For interpretation of the references to color in this figure, the reader is referred to the web version of this article.)

## 5. Conclusions

In this paper, we addressed the problem of multi-satellite scheduling with limited observation capacities, which is one of the core problems to be solved for the effective utilization of the resources of satellite constellations. The key component of our approach is the detailed analysis of possible conflicts, which leads to stronger constraints in the MILP that significantly speed up the solution process. We find that the modelling of the problem with 5-index variables (thereby avoiding the standard “Big-M” approach) is more suitable for solving real-world instances in which most variables and constraints are not necessary for the model.

In summary, for maximizing both the total number or the total weight of assigned missions, our experiments assess the correctness and effectiveness of the proposed MILP on several classes of problem instances. Good feasible solutions are obtained very fast, while the computation of true optimum solutions is also possible. The model thus provides a solid basis for designing a decision support system for scheduling satellite resources with imaging and communication tasks.

## Acknowledgments

We would like to thank the anonymous reviewers for their constructive, diligent, and detailed feedback that substantially improved the paper.

This work is supported by National Natural Science Foundation of China under Grant no.41571403, the 13th Five-year Pre-research Project of Civil Aerospace in China, Joint Funds of Equipment Pre-Research and Ministry of Education of China under Grant no.6141A02022320, and Fundamental Research Funds for the Central Universities under Grant no.CUG2017G01 and No.CUG160207.

## Appendix A. Generation of the feasible time interval

If there is a free available time window, i.e., a sub-interval of a visible time window that does not overlap with any other windows, we assign it to the corresponding mission in the preprocessing step. The remaining visible time windows of the assigned mission are ignored. Therefore, all visible time windows that remain in the model are thus overlapping with at least one other visible time window. By combining all the overlapping visible time windows of missions on the same resource, the *feasible time interval* is generated accordingly. The distributions of visible time windows and feasible time intervals are visualized in Fig. A.6.

Every resource  $R_j$  has several disjoint feasible time intervals, each consisting of pieces with a different number of overlapping visible time windows (*the conflict degree*). Fig. A.7 depicts the distribution of the conflict degree for the segments over the *feasible time intervals*. Different colors denote the different conflict degrees of segments.

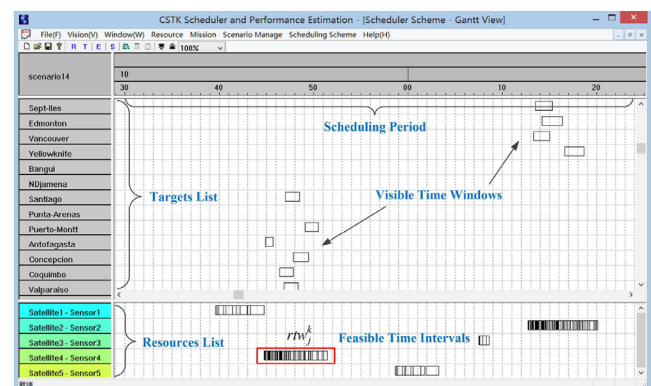


Fig. A.6. Generation and distribution of feasible time intervals.

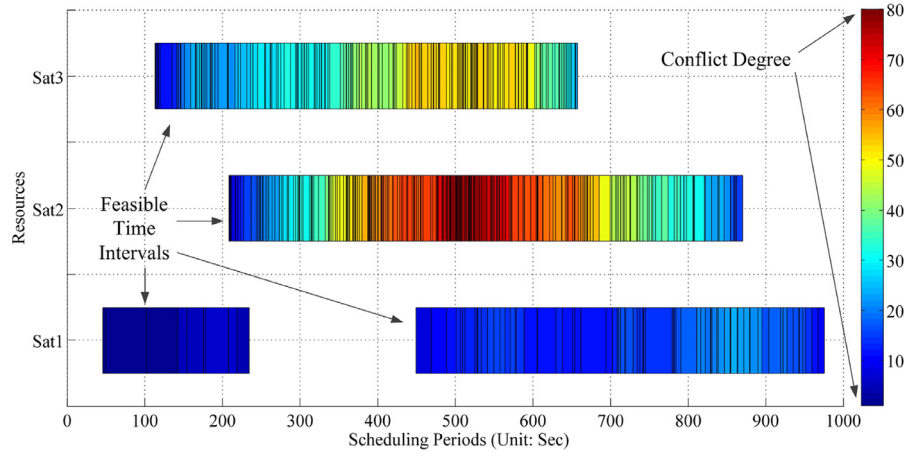


Fig. A.7. Contention conflict distribution of feasible time intervals.

## Appendix B. Calculation of effective feasible time subinterval

Since we have knowledge of all corresponding missions that can be assigned to  $srtw_j^{kl}$ , we can calculate the value of each  $srn_j^{kl}$ . If all missions have the same observation duration time  $D$ , then it can be computed as  $srn_j^{kl} = \lfloor \frac{|srtw_j^{kl}| + \delta_j}{D + \delta_j} \rfloor$ . Otherwise, we iteratively assign a mission with the shortest observation duration time by taking the setup time constraint into account until it exceeds the capacity of  $srtw_j^{kl}$  to obtain the value of  $srn_j^{kl}$ .

The generation of the *effective feasible time subinterval* is handled as follows:

- Since the value of  $srn_j^{kl}$  has already been calculated, we can perform partial assignments in a preprocessing phase. We remove the time-piece with the lowest conflict degree such that the number of the corresponding missions on  $srtw_j^{kl}$  is less than or equal to  $srn_j^{kl}$ . All corresponding missions for this interval can be assigned directly, and the search space is decreased (see Fig. B.8 (a)). We denote the remaining time subintervals as *effective feasible time subinterval*.

- Considering the distribution of conflict degrees for feasible time intervals, we include more *effective feasible time subintervals* and corresponding inequalities. To this end, we propose three operations. We iteratively “remove” a time-piece and its corresponding visible time windows according to the earliest start time, the latest end time, and the time that corresponds to the largest interval between the earliest start time and the latest end time separately (see Fig. B.8 b, c, and d).

## Appendix C. Instance analysis

In Table C.6, we show the complexity of instances and the importance of each resource based on the utilization in different types of instances with differing conflict degree and distribution. In Table C.6,  $\delta$  denotes the maximum setup time of the resource, and  $N$  is the total number of visible time windows available for each resource. The *total visible time*  $T$  is the total visibility time over all visible time windows for a resource. The *feasible observation time*  $F$  is the total time over feasible time intervals for a resource that can be assigned to missions (Due to the overlaps between visible time windows for the same resource, it is different from the *total visible*

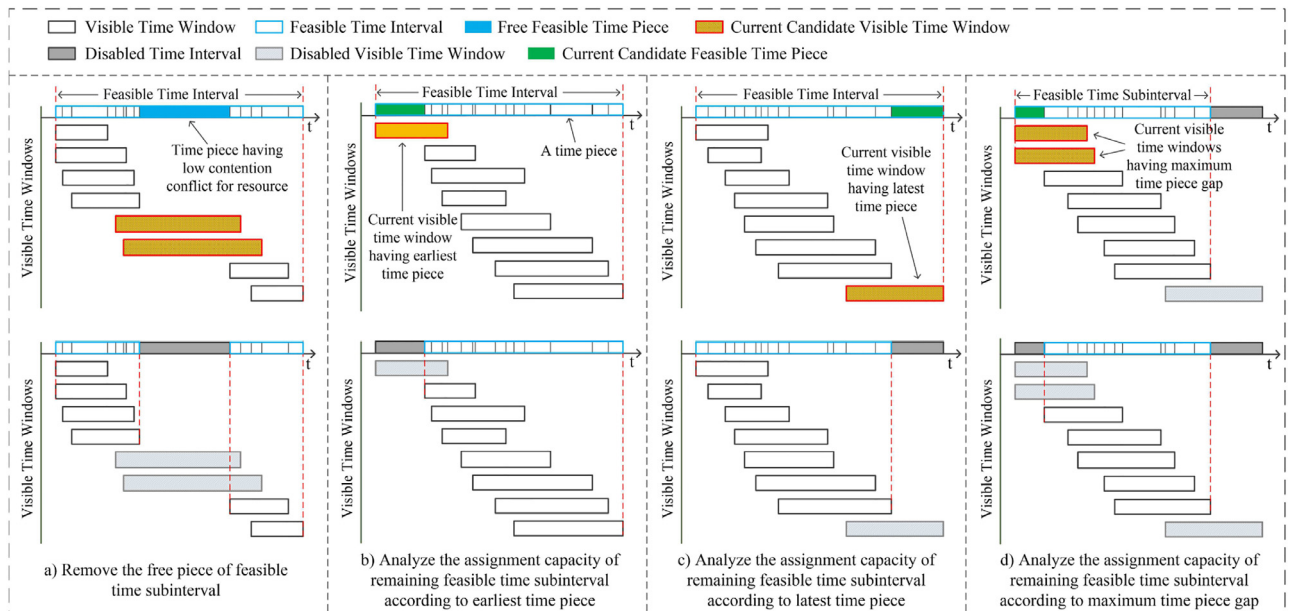


Fig. B.8. Generation of effective feasible time subintervals.

**Table C.6**  
Resource utilization.

Ins.	Sat.	Res.	$\delta(s)$	$N$	$T(s)$	$F(s)$	$m$	$conf$	$paon$	$paot$
C-1	HJ-1A	HIS	30	44	5401.56	309.74	11	16.44	1.00	99.07
	HJ-1B	IRS	30	45	4347.99	370.57	12	10.73		
	HJ-1C	SAR2	30	11	157.16	76.81	3	1.05		
C-2	HJ-1A	HSI	30	114	11692.25	1048.72	33	10.15	1.13	96.86
	HJ-1B	IRS	30	83	7225.03	1219.97	38	4.92		
	HJ-1C	SAR2	30	28	455.16	312.85	17	0.45		
C-3	HJ-1A	HSI	30	177	16966.54	1460.07	42	10.62	1.21	99.86
	HJ-1B	IRS	30	153	12466.22	1563.84	46	6.97		
	HJ-1C	SAR2	30	34	526.18	209.35	9	1.51		
C-4	HJ-1A	CCD1	40	51	5056.82	400.81	9	11.62	1.95	191.69
	HSI	30	44	5401.56	309.74	11	16.44			
	HJ-1B	CCD2	40	44	4205.78	359.60	9	10.70		
C-5	IRS	30	45	4347.99	370.57	12	10.73	2.31	202.06	
	HJ-1C	SAR2	30	11	157.16	76.81	3			1.05
	HJ-1A	CCD1	40	136	12544.85	1408.84	34			7.90
C-6	HSI	30	114	11692.25	1048.72	33	10.15	2.35	192.51	
	HJ-1B	CCD2	40	101	8493.90	1302.05	33			5.52
	IRS	30	83	7225.03	1219.97	38	4.92			
C-7	HJ-1C	SAR2	30	28	455.16	312.85	17	0.45	2.56	221.70
	HJ-1A	CCD1	40	173	14221.61	1594.25	39	7.92		
	HSI	30	177	16966.54	1460.07	42	10.62			
C-8	HJ-1B	CCD2	40	169	13573.70	1481.07	37	8.16	2.59	225.01
	IRS	30	153	12466.22	1563.84	46	6.97			
	HJ-1C	SAR2	30	34	526.18	209.35	9	1.51		
C-9	HJ-1A	CCD1	40	251	20517.75	1783.73	36	10.50	3.67	366.30
	HSI	30	251	25557.12	1930.87	45	12.24			
	HJ-1B	CCD2	40	237	20457.45	1785.02	43	10.46		
C-10	IRS	30	242	21479.04	1868.40	57	10.50	3.40	301.76	
	HJ-1C	SAR2	30	44	669.25	337.05	17			0.99
	HJ-1A	CCD1	40	287	24015.23	1686.79	37			13.24
C-11	HSI	30	302	30849.21	1881.88	50	15.39	4.34	377.97	
	HJ-1B	CCD2	40	323	27687.92	2027.46	49			12.66
	IRS	30	330	29139.61	2110.58	62	12.81			
C-12	HJ-1C	SAR2	30	53	811.56	364.61	18	1.23	4.31	376.24
	HJ-1A	CCD1	40	125	11638.60	813.02	19	13.32		
	HSI	30	88	10659.17	623.03	21	16.11			
C-13	HJ-1B	CCD2	40	71	6972.31	548.55	14	11.71	4.31	376.24
	IRS	30	72	7202.65	560.91	18	11.84			
	HJ-1C	SAR2	30	11	157.16	76.81	3	1.05		
M-1	HJ-1A	CCD1	40	253	22024.57	2223.94	55	8.90	4.34	377.97
	HSI	30	181	18953.14	1593.73	49	10.89			
	HJ-1B	CCD2	40	123	10471.08	1724.89	43	5.07		
M-2	IRS	30	95	8448.97	1463.36	44	4.77	4.31	376.24	
	HJ-1C	SAR2	30	28	455.16	312.85	17			0.45
	HJ-1A	CCD1	40	369	29721.34	2673.48	65			10.12
M-3	HSI	30	273	26917.49	1899.59	56	13.17	4.31	376.24	
	HJ-1B	CCD2	40	248	20545.92	2174.95	55			8.45
	IRS	30	182	15365.81	1851.21	55	7.30			
M-4	HJ-1C	SAR2	30	34	526.18	209.35	9	1.51	4.34	377.97
	HJ-1A	CCD1	40	543	44443.30	3975.35	86	10.18		
	HSI	30	378	38680.16	3403.81	81	10.36			
M-5	HJ-1B	CCD2	40	451	38735.80	3582.40	79	9.81	4.31	376.24
	IRS	30	321	28658.97	2717.88	80	9.54			
	HJ-1C	SAR2	30	44	669.25	337.05	17	0.99		
M-6	HJ-1A	CCD1	40	677	56901.40	3852.66	88	13.77	4.31	376.24
	HSI	30	447	45886.18	3407.96	91	12.46			
	HJ-1B	CCD2	40	569	48600.95	3898.63	89	11.47		
M-7	IRS	30	407	35921.75	3062.02	89	10.73	1.07	101.40	
	HJ-1C	SAR2	30	53	811.56	364.61	18			1.23
	HJ-1A	HIS	30	45	5138.73	567.13	14			8.06
M-8	HJ-1B	IRS	30	54	4874.60	1595.55	29	2.06	1.16	100.17
	HJ-1C	SAR2	30	8	126.23	67.39	3	0.87		
	HJ-1A	HSI	30	93	9381.23	1460.33	37	5.42		
M-9	HJ-1B	IRS	30	120	10356.08	2194.82	59	3.72	1.19	103.84
	HJ-1C	SAR2	30	18	296.09	140.49	6	1.11		
	HJ-1A	HSI	30	151	15150.84	1738.97	44	7.71		
M-10	HJ-1B	IRS	30	184	15645.23	3223.84	77	3.85	2.07	194.17
	HJ-1C	SAR2	30	22	355.19	148.52	6	1.39		
	HJ-1A	CCD1	40	43	4283.88	406.60	9	9.54		
M-11	HSI	30	45	5138.73	567.13	14	8.06	2.06	194.17	
	HJ-1B	CCD2	40	57	4994.01	1503.96	27			2.32
	IRS	30	54	4874.60	1595.55	29	2.06			
M-12	HJ-1C	SAR2	30	8	126.23	67.39	3	0.87	2.06	194.17

(continued on next page)

Table C.6 (continued)

Ins.	Sat.	Res.	$\delta(s)$	$N$	$T(s)$	$F(s)$	$rn$	$conf$	$paon$	$paot$
M-5	HJ-1A	CCD1	40	97	8688.12	1440.46	34	5.03	2.31	199.85
		HSI	30	93	9381.23	1460.33	37	5.42		
	HJ-1B	CCD2	40	134	11248.59	2111.44	51	4.33	2.39	205.43
M-6	HJ-1A	IRS	30	120	10356.08	2194.82	59	3.72		
		SAR2	30	18	296.09	140.49	6	1.11		
	HJ-1B	CCD1	40	160	13827.02	1656.37	39	7.35	2.30	194.53
M-7	HJ-1A	HSI	30	151	15150.84	1738.97	44	7.71		
		CCD2	40	199	16650.92	3098.04	66	4.37		
	HJ-1B	IRS	30	184	15645.23	3223.84	77	3.85	2.16	178.41
M-8	HJ-1A	SAR2	30	22	355.19	148.52	6	1.39		
		CCD1	40	295	24607.41	5392.2	96	3.56		
	HJ-1B	HSI	30	291	28775.26	2633.39	64	9.93	3.93	374.05
M-9	HJ-1A	CCD2	40	210	17288.81	4265.57	74	3.05		
		IRS	30	81	6485.44	3207.25	57	1.02		
	HJ-1B	SAR2	30	41	655.26	485.40	25	0.35	4.07	356.65
M-10	HJ-1A	CCD1	40	334	27847.32	6509.20	122	3.28		
		HSI	30	300	28891.38	3416.69	83	7.46		
	HJ-1B	CCD2	40	308	24596.35	6820.68	126	2.61	4.17	361.57
M-11	HJ-1A	IRS	30	93	7146.66	3298.15	62	1.17		
		SAR2	30	45	721.53	573.52	30	0.26		
	HJ-1B	CCD1	40	121	11012.80	776.74	19	13.18	3.99	339.35
M-12	HJ-1A	HSI	30	90	10397.46	982.28	27	9.59		
		CCD2	40	90	8094.21	2825.45	47	1.86		
	HJ-1B	IRS	30	84	7774.62	2883.95	48	1.70	4.07	347.95
M-13	HJ-1A	SAR2	30	8	126.23	67.39	3	0.87		
		CCD1	40	281	23817.80	3359.23	80	6.09		
	HJ-1B	HSI	30	170	17551.99	2243.98	56	6.82	1.31	107.36
R-1	HJ-1A	CCD2	40	201	17003.69	3642.71	85	3.67		
		IRS	30	144	12660.71	2902.44	74	3.36		
	HJ-1B	SAR2	30	18	296.09	140.49	6	1.11	1.28	105.77
R-2	HJ-1A	CCD1	40	407	33683.82	3623.79	87	8.30		
		HSI	30	255	25859.69	2577.14	65	9.03		
	HJ-1B	CCD2	40	332	27988.76	5624.21	114	3.98	1.26	101.96
R-3	HJ-1A	IRS	30	236	20582.38	4786.82	103	3.30		
		SAR2	30	22	355.19	148.52	6	1.39		
	HJ-1B	CCD1	40	524	43726.61	9351.85	165	3.68	2.43	200.96
R-4	HJ-1A	HSI	30	479	47108.39	5264.96	122	7.95		
		CCD2	40	423	34216.82	7741.70	142	3.42		
	HJ-1B	IRS	30	127	10015.32	5094.58	94	0.97	2.47	205.99
R-5	HJ-1A	SAR2	30	42	673.92	504.06	26	0.34		
		CCD1	40	667	56629.50	14082.51	258	3.02		
	HJ-1B	HSI	30	576	56857.17	9312.37	206	5.11	2.44	200.60
R-6	HJ-1A	CCD2	40	575	46201.02	13102.91	238	2.53		
		IRS	30	172	13566.61	7074.17	128	0.92		
	HJ-1B	SAR2	30	45	721.53	573.52	30	0.26	1.31	107.36
R-7	HJ-1A	CCD1	40	170	17219.78	7210.43	118	1.39		
		HSI	30	166	14165.54	5382.46	94	1.63		
	HJ-1B	IRS	30	11	116.99	116.99	11	0.00	1.28	105.77
R-8	HJ-1A	SAR1	25	11	116.99	116.99	11	0.00		
		SAR2	30	46	706.49	653.70	39	0.08		
	HJ-1B	HSI	30	210	21363.18	8508.24	142	1.51	1.26	101.96
R-9	HJ-1A	IRS	30	231	19933.08	9559.21	152	1.09		
		SAR1	25	12	126.75	126.75	12	0.00		
	HJ-1B	SAR2	30	57	883.27	777.86	47	0.14	1.28	105.77
R-10	HJ-1A	CCD1	40	170	14257.38	6755.10	112	1.11		
		HSI	30	170	17219.78	7210.43	118	1.39		
	HJ-1B	CCD2	40	166	13822.88	5239.04	86	1.64	2.43	200.96
R-11	HJ-1A	IRS	30	166	14165.54	5382.46	94	1.63		
		SAR1	25	11	116.99	116.99	11	0.00		
	HJ-1B	SAR2	30	46	706.49	653.70	39	0.08	2.47	205.99
R-12	HJ-1A	CCD1	40	245	20460.47	10263.72	171	0.99		
		HSI	30	210	21363.18	8508.24	142	1.51		
	HJ-1B	CCD2	40	234	19627.92	9203.93	142	1.13	2.44	200.60
R-13	HJ-1A	IRS	30	231	19933.08	9559.21	152	1.09		
		SAR1	25	12	126.75	126.75	12	0.00		
	HJ-1B	SAR2	30	57	883.27	777.86	47	0.14	2.44	200.60
R-14	HJ-1A	CCD1	40	298	24794.29	12754.80	221	0.94		
		HSI	30	247	24748.59	10327.56	179	1.40		
	HJ-1B	CCD2	40	291	24523.34	12205.38	199	1.01	2.44	200.60
R-15	HJ-1A	IRS	30	285	24789.20	12415.51	205	1.00		
		SAR1	25	20	211.59	204.68	18	0.03		
	HJ-1B	SAR2	30	79	1233.10	1062.72	63	0.16		

(continued on next page)

Table C.6 (continued)

Ins.	Sat.	Res.	$\delta(s)$	$N$	$T(s)$	$F(s)$	$m$	$conf$	$paon$	$paot$
R-7	HJ-1A	CCD1	40	394	32805.30	15058.92	272	1.18	2.62	218.61
		HSI	30	359	35980.50	13316.92	252	1.70		
	HJ-1B	CCD2	40	378	31809.02	14261.62	247	1.23		
		IRS	30	332	28953.59	12883.02	224	1.25		
	HJ-1C	SAR1	25	21	220.32	213.41	19	0.03		
		SAR2	30	89	1394.67	1178.06	71	0.18		
R-8	HJ-1A	CCD1	40	468	39119.41	17147.12	315	1.28	2.72	228.59
		HSI	30	449	44694.12	15967.84	312	1.80		
	HJ-1B	CCD2	40	492	41659.75	17020.37	310	1.45		
		IRS	30	374	32698.60	13032.66	229	1.51		
	HJ-1C	SAR1	25	23	239.07	232.16	21	0.03		
		SAR2	30	101	1602.63	1326.67	79	0.21		
R-9	HJ-1A	CCD1	40	597	49603.80	20593.61	395	1.41	2.88	241.49
		HSI	30	538	53486.70	19275.32	384	1.77		
	HJ-1B	CCD2	40	620	51972.71	20314.63	384	1.56		
		IRS	30	416	36115.20	14705.63	265	1.46		
	HJ-1C	SAR1	25	25	258.94	252.03	23	0.03		
		SAR2	30	111	1758.41	1478.82	88	0.19		
R-10	HJ-1A	CCD1	40	666	55439.42	23101.46	443	1.40	2.86	237.52
		HSI	30	578	57447.53	20896.70	415	1.75		
	HJ-1B	CCD2	40	696	58559.76	22731.15	435	1.58		
		IRS	30	459	39784.35	16460.32	303	1.42		
	HJ-1C	SAR1	25	30	307.84	300.93	28	0.02		
		SAR2	30	141	2230.07	1889.91	113	0.18		
R-11	HJ-1A	CCD1	40	783	65837.40	24557.99	477	1.68	2.92	244.30
		HSI	30	657	65689.49	22099.31	444	1.97		
	HJ-1B	CCD2	40	784	65688.80	23582.36	452	1.79		
		IRS	30	511	44351.37	17214.34	320	1.58		
	HJ-1C	SAR1	25	33	343.53	336.61	31	0.02		
		SAR2	30	150	2385.59	2008.28	118	0.19		

time. Instead, it corresponds to the union of the overlapping visible time windows of a resource).

### Supplementary material

Supplementary material associated with this article can be found, in the online version, at doi:[10.1016/j.ejor.2018.11.058](https://doi.org/10.1016/j.ejor.2018.11.058).

### References

- Barbulescu, L., Watson, J. P., & Whitley, L. D. (2004). Scheduling space-ground communications for the Air Force satellite control network. *Journal of Scheduling*, 7(1), 7–34.
- Bensana, E., Lemaître, M., & Verfaillie, G. (1999). Earth observation satellite management. *Constraints*, 4(3), 293–299.
- Bianchessi, N., Cordeau, J. F., Desrosiers, J., Laporte, G., & Raymond, V. (2007). A heuristic for the multi-satellite, multi-orbit and multi-user management of Earth observation satellites. *European Journal of Operational Research*, 177(2), 750–762.
- Bianchessi, N., & Righini, G. (2008). Planning and scheduling algorithms for the cosmo-skymed constellation. *Aerospace Science and Technology*, 12(7), 535–544.
- Bonissone, P. P., Subbu, R., Eklund, N., & Kiehl, T. R. (2006). Evolutionary algorithms + domain knowledge = real-world evolutionary computation. *IEEE Transactions on Evolutionary Computation*, 10(3), 256–280.
- Cheng, T. C. E., Ng, C. T., & Yuan, J. J. (2008). Multi-agent scheduling on a single machine with max-form criteria. *European Journal of Operational Research*, 188(2), 603–609.
- Cordeau, J. F., & Laporte, G. (2005). Maximizing the value of an Earth observation satellite orbit. *Journal of the Operational Research Society*, 56(8), 962–968.
- Dilkina, B., & Havens, B. (2005). Agile satellite scheduling via permutation search with constraint propagation. *Technical Report*. Actenum Corporation.
- Gabrel, V. (2006). Strengthened 0–1 linear formulation for the daily satellite mission planning. *Journal of Combinatorial Optimization*, 11(3), 341–346.
- Gabrel, V., & Vanderpooten, D. (2002). Enumeration and interactive selection of efficient paths in a multiple criteria graph for scheduling an Earth observing satellite. *European Journal of Operational Research*, 139(3), 533–542.
- Habet, D., Vasquez, M., & Vimont, Y. (2010). Bounding the optimum for the problem of scheduling the photographs of an agile Earth observing satellite. *Computational Optimization and Applications*, 47(2), 307–333.
- Jang, J., Choi, J., Bae, H. J., & Choi, I. C. (2013). Image collection planning for Korea Multi-Purpose SATellite-2. *European Journal of Operational Research*, 230(1), 190–199.
- Lemaître, M., Verfaillie, G., Jouhaud, F., Lachiver, J., & Bataille, N. (2002). Selecting and scheduling observations of agile satellites. *Aerospace Science and Technology*, 6(5), 367–381.
- Lin, W., Liao, D., Liu, C., & Lee, Y. (2005). Daily imaging scheduling of an Earth observation satellite. *IEEE Transactions on Systems, Man and Cybernetics*, 35(2), 213–223.
- Liu, X., Bai, B., Chen, Y., & Yao, F. (2014). Multi satellites scheduling algorithm based on task merging mechanism. *Applied Mathematics and Computation*, 230, 687–700.
- Liu, X., Laporte, G., Chen, Y., & He, R. (2017). An adaptive large neighborhood search metaheuristic for agile satellite scheduling with time-dependent transition time. *Computers & Operations Research*, 86, 41–53.
- Luo, K., Wang, H., Li, Y., & Li, Q. (2017). High-performance technique for satellite range scheduling. *Computers & Operations Research*, 85, 12–21.
- Mansour, M. A. A., & Dessouky, M. M. (2010). A genetic algorithm approach for solving the daily photograph selection problem of the spot5 satellite. *Computers & Industrial Engineering*, 58(3), 509–520.
- Mao, T., Xu, Z., Hou, R., & Min, P. (2012). Efficient satellite scheduling based on improved vector evaluated genetic algorithm. *Journal of Networks*, 7(3), 517–523.
- Niu, X., Tang, H., Wu, L., Deng, R., & Zhai, X. (2015). Imaging-duration embedded dynamic scheduling of Earth observation satellites for emergent events. *Mathematical Problems in Engineering*, 2015.
- Ribeiro, G. M., Constantino, M. F., & Lorena, L. A. N. (2010). Strong formulation for the spot 5 daily photograph scheduling problem. *Journal of Combinatorial Optimization*, 20(4), 385–398.
- Salman, A. A., Ahmad, I., & Omran, M. G. H. (2015). A metaheuristic algorithm to solve satellite broadcast scheduling problem. *Information Sciences*, 322, 72–91.
- Spangelo, S., Cutler, J., Gilson, K., & Cohn, A. (2015). Optimization-based scheduling for the single-satellite, multi-ground station communication problem. *Computers & Operations Research*, 57, 1–16.
- Sun, B., Wang, W., Xie, X., & Qin, Q. (2010). Satellite mission scheduling based on genetic algorithm. *Kybernetes*, 39(8), 1255–1261.
- Tangpattanakul, P., Nicolas, J., & Pierre, L. (2015). A multi-objective local search heuristic for scheduling Earth observations taken by an agile satellite. *European Journal of Operational Research*, 245(2), 542–554.
- Vasquez, M., & Hao, J. K. (2001). A logic-constrained knapsack formulation and a tabu search algorithm for the daily photograph scheduling of an Earth observation satellite. *Computational Optimization and Applications*, 20(2), 137–157.
- Vasquez, M., & Hao, J. K. (2003). Upper bounds for the SPOT 5 daily photograph scheduling problem. *Journal of Combinatorial Optimization*, 7(1), 87–103.
- Wang, J., Zhu, X., Yang, L. T., Zhu, J., & Ma, M. (2015). Towards dynamic real-time scheduling for multiple Earth observation satellites. *Journal of Computer and System Sciences*, 81(1), 110–124.
- Wang, M., Dai, G., & Vasile, M. (2014). Heuristic scheduling algorithm oriented dynamic tasks for imaging satellites. *Mathematical Problems in Engineering*, 2014.
- Wang, P., Reinelt, G., Gao, P., & Tan, Y. (2011). A model, a heuristic and a decision support system to solve the scheduling problem of an Earth observing satellite constellation. *Computers & Industrial Engineering*, 61(2), 322–335.
- Wolfe, W. J., & Sorensen, S. E. (2000). Three scheduling algorithms applied to the Earth observing systems domain. *Management Science*, 46, 148–168.



- Wu, G., Liu, J., Ma, M., & Qiu, D. (2013). A two-phase scheduling method with the consideration of task clustering for Earth observing satellites. *Computers & Operations Research*, 40(7), 1884–1894.
- Wu, G., Ma, M., Zhu, J., & Qiu, D. (2012). Multi-satellite observation integrated scheduling method oriented to emergency tasks and common tasks. *Journal of Systems Engineering and Electronics*, 23(5), 723–733.
- Xhafa, F., Herrero, X., Barolli, A., Barolli, L., & Takizawa, M. (2013). Evaluation of struggle strategy in genetic algorithms for ground stations scheduling problem. *Journal of Computer and System Sciences*, 79(7), 1086–1100.
- Xhafa, F., Sun, J., & Barolli, A. (2012). Genetic algorithms for satellite scheduling problems. *Mobile Information Systems*, 8(4), 351–377.
- Xiong, J., Leus, R., & Yang, Z. (2016). Evolutionary multi-objective resource allocation and scheduling in the Chinese navigation satellite system project. *European Journal of Operational Research*, 251(2), 662–675.
- Xu, Y., Xu, P., Wang, H., & Peng, Y. (2010). Clustering of imaging reconnaissance tasks based on clique partition. *Operations Research and Management Science*, 19(4), 143–149.
- Yao, F., Li, J., Bai, B., & He, R. (2010). Earth observation satellites scheduling based on decomposition optimization algorithm. *International Journal of Image, Graphics and Signal Processing*, 2(1), 10–18.
- Zhang, Z., Zhang, N., & Feng, Z. (2014). Multi-satellite control resource scheduling based on ant colony optimization. *Expert Systems with Applications*, 41(6), 2816–2823.